Elovanoid-N32 or RvD6-isomer decrease ACE2 and binding of S protein RBD after injury or INFγ in the eye

Thang L. Pham
  Louisiana State University Health New Orleans

Jiucheng He
  Louisiana State University Health New Orleans

Azucena H. Kakazu
  Louisiana State University Health New Orleans

Jorgelina Calandria
  Louisiana State University Health New Orleans

Khanh V. Do
  Louisiana State University Health New Orleans

Robert Nshimiyimana
  University of Southern California

Nicos A. Petasis
  University of Southern California

Haydee E.P. Bazan (✉ HBazan1@lsuhsc.edu)
  Louisiana State University Health New Orleans   https://orcid.org/0000-0001-7172-7870

Nicolas G. Bazan (✉ nbazan@lsuhsc.edu)
  Louisiana State University Health New Orleans   https://orcid.org/0000-0002-9243-5444

Abstract

The severe acute respiratory syndrome coronavirus 2 (SARS-CoV-2) infection that causes coronavirus disease 2019 (COVID-19) has resulted in a pandemic affecting the most vulnerable in society, triggering a public health crisis and economic tall around the world. Effective treatments to mitigate this virus infection are needed. Since the eye is a route of virus entrance, we use an *in vivo* rat model of corneal inflammation as well as human corneal epithelial cells in culture challenged with IFNγ to study this issue. We explore ways to block the receptor-binding domain (RBD) of SARS-CoV-2 spike (S) protein to angiotensin-converting enzyme 2 (ACE2). Elovanoid (ELV)-N32 or Resolvin D6-isomer (RvD6i), among the lipid mediators studied, consistently decreased the expression of the ACE2 receptor, furin, and integrins in damaged corneas or IFNγ stimulated human corneal epithelial cells (HCEC). There was also a concomitant decrease in the binding of spike RBD with the lipid treatments. Concurrently, we uncovered that the lipid mediators also attenuated the expression of cytokines that participate in the cytokine storm, hyper-inflammation and senescence programming. Thus, the bioactivity of these lipid mediators will contribute to opening therapeutic avenues for COVID-19 by counteracting virus attachment and entrance to the eye and other cells and the ensuing disruptions of homeostasis.

Introduction

In December 2019, a new infectious respiratory disease (Coronavirus disease 2019, COVID-19[1]) caused by severe acute respiratory syndrome coronavirus 2 (SARS-CoV-2) emerged[2,3], quickly becoming a pandemic and a global threat to public health. The virus has a single-stranded RNA with a 30 kb genome, which encodes the spike (S) protein that expresses a receptor-binding domain (RBD) for the angiotensin-converting enzyme 2 (ACE2) receptor[4]. In addition, S protein contains cleavage sites for cell proteases FURIN and transmembrane serine protease 2 (TMPRSS2) that allow viral cell entrance[5]. Cells from the alveoli, GI tract, and cornea epithelium, among others, co-expressed *Ace2* and *Tmprss2* genes[6].

The eye surface, particularly the cornea, is a route of SARS-CoV-2 entrance[6,7]. Also, the nasolacrimal duct could leak virus-containing tears into the upper respiratory tract. Several lipid mediators modulate inflammatory responses and have been hypothesized to counteract COVID-19 pathology[8,9]. Lipid mediators facilitate debris clearance and antagonize pro-inflammatory cytokines by fostering inflammation resolution[10,11]. Here, we study lipoxin A4 (LXA4) derived from the ω-6 arachidonic acid[12], the R,R stereoisomers Neuroprotectin D1 (NPD1)[13] and Resolvin D6-isomer (RvD6i)[14] called docosanoids since they are derived from ω-3 docosahexaenoic acid and Elovanoid (ELV)-N32 that belongs to a new lipid mediator class discovered in our laboratory – the elovanoids[15,16]. These lipids are di-hydroxylated derivatives of very long chain polyunsaturated fatty acids (>28C, VLC-PUFAs) with pro-homeostatic and neuroprotective bioactivity[11,15,16]. Here, we show that ELV-N32 and RvD6i selectively decrease ACE2 receptor expression and binding of RBD of the S protein in the cornea stroma in an *in vivo* rat model of cornea injury. We confirm that *Ace2* is an interferon-stimulated gene in HCEC, a mechanism that would enhance SARS-CoV-2 infectivity[17]. Therefore, we use HCEC in culture challenged with IFNγ to

demonstrate that ELV-N32 or RvD6i exert blockage of ACE2 receptor expression, binding of RBD, hyper-inflammation, senescence programming, and components of the cytokine storm.

Results

Lipid mediators decrease cornea injury-induced expression of ACE2 and binding of Alexa 594- RBD.

Host proteases for S protein: FURIN5, TMPRSS2 and dipeptidyl peptidase 4 (DPP4)18 are expressed in the cornea (Fig. 1**a**), indicating that it is a potential site for SARS-CoV-2 entrance, in agreement with clinical studies showing infected patients' epiphora, conjunctival congestion, or chemosis19. SARS-CoV-2 triggers lung injury and a systemic dysfunction of the inflammatory-immune system reflected in the cytokine storm20,21. We found that our cornea injury model recapitulates inflammatory-immune system dysfuctions22, including ACE2 receptor expression upon injury. To identify mediators that modulate these responses and to understand consequent mechanisms, we tested the following lipid mediators: LXA4, ELV-N32, RvD6i, and NPD1 (Fig. 1**b,c**). LXA4, ELV-N32, and RvD6i decrease ACE2 abundance and gene expression levels (Supplementary Fig. S**1**) to non-injured tissue, while NPD1 had no effect (Fig. 1**d**). Alexa 594-RBD displayed remarkable binding to injured cornea stroma, and LXA4, ELV-N32, and RvD6i counteracted these injury-induced effects. Again, NPD1 did not have an effect. Thus, there is a correlation between changes in the ACE2 receptor and RBD binding in the cornea after injury and lipid treatment. Interestingly, most of the RBD was detected in the stroma, and inflammatory cells labeled with CD68 showed co-localization with RBD (Supplementary Fig. S2**a-b**).

Lipid mediators disrupt the ACE2 upregulation, hyper-inflammation, senescence, and cytokine storm components in the injured cornea *in vivo*.

RNA-seq analysis 14 days after injury with and without treatment (Fig. 1**b**) revealed well-clustered transcriptional profiles in each treated group (Fig. 2**a**). In PCA plots, the transcriptomic profile of non-injured corneas, control (red), and injured corneas treated with vehicle (green) were well separated. Topical treatment with lipid mediators shows profiles closer to control corneas than to vehicle-treated corneas. ELV-N32 (pink) and RvD6i (cyan) were the nearest to the normal cornea. DEseq2 analysis allows comparison of all treated groups as well as control corneas to vehicle as a reference. Upregulated genes in vehicle-treated injury corneas revealed differences among treatment with lipid mediators, as depicted in Venn diagrams (Fig. 2**b**). Since NPD1 failed to decrease the ACE2 expression and RBD binding upon injury (Fig. 1**d-h**), we focused on the groups of shared genes between control-LXA4-ELV- N32-RvD6i (450 genes including *Ace2*) and control-ELV-N32-RvD6i (737 genes). KEGG pathway analysis of these two data sets revealed cytokines and senescence-related pathways (Fig. 2**c**) with significant false discover rate (FDR) values. On the other hand, IPA analysis predicted several cytokines as upstream regulators of Ace2 increased expression after injury. Interestingly, in addition to cytokines, the CDKN2A (p16/INK4) and NFkB (complex) and its correlated genes were predicted as inducers of *Ace2* (Fig. 2**d**). The RNA-seq analysis of *Cdkn2a* gene (Fig. 2**e**) and the IPA inhibition score and p-value of this gene (Fig. 2**f**) and the NFKB complex (Fig. 2**g**) confirm the prediction.

Lipid mediators counter-regulate cytokine storm components, NFkB/inflammation, and senescence-associated secretory phenotype after cornea injury.

Since *Ace2* gene activation is caused by the action of cytokines, p16INK4a and NFkB, we targeted genes regulated by those inducers. Thus, we explored in the injured cornea: (i) activated cytokines found in the serum of SARS-CoV-2 patients20, (ii) senescence-associated secretory phenotype (SASP) genes23, and (iii) NFkB/inflammation genes found in lung biopsies of SARS-CoV-224. The Venn diagram showed several shared genes by the three inducers (Fig. 3**a**). Fifty-one injury-upregulated genes were counteracted by the lipid mediators (Fig. 3**b**). The plot for each specific gene is provided in Supplementary Figs. S3- Among those genes, *Cxcl10*, *Hgf*, and *Il1r1* (Supplementary Figs. S3**c**, S4 and S5) are related to SARS-CoV-2 load25, while metalloproteinases related genes, such as *Mmp9* (Supplementary Fig. S4), *Mmp3*, *Mmp12*, and *Timp1* (Supplementary Fig. S5) are increase after coronavirus infection and involved in degradation of the extracellular matrix, which facilitates hyperinflammation, leukocyte infiltration, and ECM remodeling and fibrosis26,27. Further, transient receptor *Trpc6* (Supplementary Fig. S4) is a component of chronic obstructive pulmonary disease development28.

Using the KEGG pathway analysis, we found similar pathways to those found in the entire transcriptome (Fig. 2**c** and Supplementary Fig. S3**a**). Employing the EnrichR – Archs4 human analysis tissue database, the 51 genes are more abundant in the omentum and lung (bulk tissue) (Fig. 3**c**). This suggests that genes detected in the injured cornea might recapitulate changes in gene expression that occur in lung injury. Three targeted cytokines *Il1b*, *Il6*, and *Vegfa* genes are plotted in Fig. 3**d**. Our data showed that *Il6* and *Vegfa* were upregulated by the injury, and the administration of LXA4, ELV-N32, or RvD6i reduced their expression (Fig. 3**d**). We also focused on integrin genes since the spike protein contains an RGD motif in the RBD site that is recognized by some integrins as a potential receptor of SARS-CoV-229,30. Six integrins, which have the RGD binding domain in the heterodimer confirmation, are increased after injury and decreased by some of the lipid mediators (Fig. 3**e**). Among these genes, *Itga5* and *Itgb1* are of interest since their specific blocker ATN-161 greatly attenuates the SARS-CoV-2 infection *in vitro*31, and their expression is significantly decreased by ELV-N32 and RvD6i.

Lipid mediators attenuate IFNγ-specific induction of ACE2 expression, Alexa 594-RBD binding, and senescence programming in human corneal epithelial cells.

Based on the IPA prediction of upstream regulators of *Ace2* targeted cytokines, we treated HCEC with IL1β, IL2, IL6, IL8, IFNγ, IFNα, IFNε or TNFα at 1, 10, and 100 ng/mL. IFNγ or IFNα were the only cytokines to activate *Ace2* expression, with IFNγ being the more potent of the two (Fig. 4**a** and Supplementary Fig. S6). We followed *Ace2* expression by dd-PCR that provides absolute quantification. ELV-N32 or RvD6i markedly attenuated IFNγ-triggered *Ace2* activation (Fig. 4**b**). In addition, IFNγ stimulates the overexpression of senescence programming genes *Cdkn2a* (p16INK4a) and *Mmp1*. ELV- N32, RvD6i, and NPD1 decrease *Cdkn2a* activation to control values, but LXA4 does not. IFNγ- stimulated Alexa 594-RBD binding (Fig. 4**c**) correlates with increased ACE2 expression (Fig. 4**b**). ELV- N32, RvD6, and NPD1 decrease IFNγ-stimulated RBD binding (Fig. 4**c**). Therefore, our data show that following IFNγ-stimulated RBD

binding to ACE2, induction of senescence programming genes *Cdkn2a* (p16INK4a) and *Mmp1* as well as SASP secretome activation takes place. These events are blocked by ELV-N32, RvD6i, and NPD1 but not by LXA4 (Fig. 4**d**).

Discussion

Here, we discern bioactivity among a group of lipid mediators on critical targets related to SARS-CoV-2 entrance and deleterious consequences of this viral infection. We uncover that the lipid mediators ELV-N32 and RvD6i decrease ACE2 receptor expression, binding of RBD of the S protein, inflammatory responses, and senescence programming using the rat cornea *in vivo* model. In addition, we demonstrate using HCEC in culture challenged with IFNγ that ELV-N32 and RvD6i exert similar effects. ELV-N32 remarkably decreases Furin expression, a protease that cleaves the S1/S2 site required for SARS-CoV-2 entry in lung cells[5].

A key cytokine responding to viral infections is IFNγ[32] that increases in the serum of severely affected COVID-19 patients[20,33]. We found that IFNγ induces *Ace2* expression in HCEC at a much lower dose than INFα. Moreover, IFNγ activates cellular senescence reflected in enhanced *Cdkn2a* expression and SASP secretome release. This observation could contribute to explain why aging populations are more susceptible to COVID-19[34]. ELV-N32 does bear senolytic activity[16], and both, ELV-N32 and RvD6i suppressed senescence genes and the SASP secretome in HCEC (Fig. 4**d**). Therefore, S protein internalization may lead to IFNγ secretion, which would synergize with an integrin-rich environment amplifying the IFNγ effect[35] and stimulating *Ace2* overexpression. As a result, the higher ACE2, the higher SARS-CoV-2 binding would be possible. ELV-N32 and RvD6i suppressed the IFNγ stimulation of *Ace2* expression as well as the IFNγ-induced senescence, where many SASP components are pro-inflammatory cytokines. PEDF+DHA (the precursor of RvD6i) and RvD1 suppress type 1 pro-inflammatory macrophages (induced by IFNγ) while increasing the type 2 anti-inflammatory macrophage phenotype[36,37]. Interestingly, ELV-N32, RvD6i, and NPD1 attenuated ACE2-RBD in the IFNγ-treated cells in culture (Fig. 4**c**), while in the rat injured cornea, LXA4 displayed a significant effect on preventing ACE2-RBD interaction (Fig. 1**f-h**). Of the lipid mediators studied, ELV-N32 and RvD6i consistently displayed protective bioactivity. RvD6i was recently identified in mouse tears as related to corneal nerve regeneration[14,38]. ELV-N32 is a powerful neuroprotective and anti-inflammatory lipid mediator[16].

ELV-N32 and RvD6i also decrease integrins expression. The S protein contains an RGD motif in the RBD site that recognizes integrins and stimulates virus internalization by activation PI-3K, a pathway predicted to increase along with ACE2 enhanced expression (Fig. 2**c**)[29,30]. Inhibition of integrin α5β1 by a non-RGD peptide derived from fibronectin, inhibit the binding of the S protein to ACE2 and decrease virus infection in *in vitro*[31].

In conclusion, our data demonstrate that ELV-N32 or RvD6i diminish ACE2 expression and binding of the S protein RBD and, consequently, activate pro-homeostatic signaling and reduce tissue damage.

The application of these lipid mediators could be of therapeutic use alone or as a complement with current antiviral strategies for COVID-19. Moreover, the lipid mediators identified here might work by similar mechanisms in other cell types and further expand the scope of their therapeutic applications beyond the eye.

Limitations of this study.

Additional research will be needed to fully elucidate the molecular mechanisms used by the lipid mediators that elicit downregulation of ACE2 and the genes encoding inflammatory/senescence proteins. The use of the entire S protein in the models studied here will provide the connection between lipid mediators acting on cell attachment and cell entrance, particularly since ELV-N32 remarkably reduces furin expression correlated with ACE2 downregulation. Moreover, the use of the intact virus would offer a direct demonstration of the significance of the effects of the lipid mediators studied here.

Methods

Animals

Sprague-Dawley rats (8-week-old male) were obtained from Charles River Laboratories (Wilmington, MA, USA) and kept at the Animal Care of the Neuroscience Center of Excellence, Louisiana State University Health (LSUH; New Orleans, LA, USA). All animals were handled in compliance with the guidelines of the ARVO Statement for the Use of Animals in Ophthalmic and Vision Research, and the experimental protocol was approved by the Institutional Animal Care and Use Committee (IACUC) at LSUH.

Cornea Injury

The rats were anesthetized by intraperitoneal injection of Ketamine (50-100 mg/kg) plus xylazine (5-10 mg/kg). A 4 mm diameter filter paper soaked in 1 N NaOH was placed on the central cornea of the right eye for 45 seconds, and then the eye was thoroughly washed with 10 mL of saline. After injury, the rats were randomly divided into five treatment groups: vehicle; lipoxin A4 (LXA4) from Cayman Chemical (Ann Arbor, MI, USA); R,R Resolvin D6 isomer (RvD6i), R,R neuroprotection D (NPD1), and elovanoid (ELV)-N32 synthesized by Dr. R. Nshimiyimana and Prof. N. Petasis. All lipid solutions were prepared at the final concentration of 10 µM using PBS with the minimal contamination of ethanol by evaporating the ethanol and immediately dissolve the lipids in PBS, then vortex well for 2 min. Topical administration (20 µl) was done 3x/day for 14 days. The experiments were double-blinded with the lipid mediators coded during the whole experiments. At the end of the study, when all data was collected, the code was opened.

Corneal RNA-sequencing

Injured corneas (n = 5/condition) were harvested and homogenized with TRIzol (Thermo Fisher Scientific) on ice with a glass Dounce homogenizer. RNA sequencing was performed as described14. Briefly, after mRNA extraction and determination of purity, 8 ng of total RNA was reverse transcribed, and total cDNAs were amplified using ISPCR primer, and the library was made with the Nextera XT DNA library preparation

kit (Illumina, San Diego, CA, USA). The libraries were pooled with the same molarity and sequenced using the NextSeq 500/550 High Output Kit v2 (75 cycles, Illumina). After demultiplexing, RNA-seq data were aligned to the Rattus Norvegicus reference genome (ftp://ftp.ensembl.org/pub/release-98/fasta/rattus_norvegicus/dna/) using the Subread package v2.0.1 alignment function[39]. The BAM files for sequencing data alignment were counted using featureCounts function of Subread tool[40] using the macOS Catalina. The raw count data were subjected to differential gene expression analysis using DESeq2 package for R[41] with the vehicle group as reference. The adjusted p-values were named as the false discover rate (FDR). Significantly changed genes (FDR < 0.05) between each treatment vs. vehicle were subjected to the enrichment analysis using EnrichR[42] and NetworkAnalyst 3.0[43], and pathway analysis using the IPA (QIAGEN Inc., https://www.qiagenbioinformatics.com/products/ingenuity-pathway-analysis).

Preparation of Alexa 594-conjugated RBD fragment of S protein

RBD fragment of the Spike protein belonging to SARS-CoV-2 (Raybiotech, Peachtree Corners GA. Cat. 230-30162-1000) was labeled using Alexa Fluor™ 594 Protein Labeling Kit (ThermoFisher, Waltham, MA. Cat. A10239) following the manufacturer's directions. Briefly, 1 mg of protein was dissolved in 0.1 M bicarbonate and then incubated with the Alexa Fluor 594 dye for one hour. The dye was washed using an Amicon-Ultra centrifugal filter cutoff 10KDa (Merck, Millipore Carrigtwohill, CO. Cat. UFC201024). To assess the efficiency of the label, the protein was measured at 280 nm and 590 nm absorbance using NanoDrop One (Thermo Scientific). There was a ratio of 0.4 moles of dye/mole of protein and a recovery of about 80%.

Human corneal epithelial cells (HCEC) culture

All experiments with human corneal epithelial cells were approved by the Institutional Review Board of LSUHNO and conducted in accordance with NIH guidelines. HCEC were kept frozen in the laboratory at passage 25[44]. Cells were maintained in keratinocyte growth (KGM) medium containing the keratinocyte basal medium (KBM) (Lonza: CC-3101) supplemented with bovine pituitary extract (BPE), hEGF, Insulin, Hydrocortisone and Gentamicin Sulfate-Amphotericin (GA-1000) (Lonza, Cat. CC-4131). For all experiments, cells were seeded at 30,000 cells/cm2.

For screening the stimulation of receptor ACE2 by cytokines, the HCEC were cultured with KGM until 50-60% confluence. Then, changed to KBM containing IL-1β, -2, -6 and 8, IFN-α, -ε, and -γ or TNFα at 1, 10 or 100 ng/ml. The cells were harvested after 6 hours and analyze for the gene expression of *Ace2*. In other experiments, HCEC were stimulated with IFNγ, and thereafter, lipid mediators were added. For the Alexa 594-conjugated RBD binding, IFNγ was used as a cytokine trigger. At 12 hours after cytokine exposure and lipid mediator treatments, 0.5 µg of labeled RBD was added to the medium. The evaluation of RBD binding was conducted 24 hours after.

Immunohistochemistry

Corneal tissue was fixed in Zamboni fixative (MasterTech Scientific, Lodi, CA USA) for 2 hours immediately after euthanasia. After thoroughly washing with PBS, the corneas were embedded in optimal cutting temperature compound, and serial 10-μm cryostat sections were obtained, dried at room temperature for 2 hours, and stored at -20 °C until use. For immunofluorescence, the sections were incubated with primary antibodies at the concentration described in Table 1 in a wet chamber at 4 °C overnight. The sections were washed 3 x/5 min with PBS following by incubation for 1 hour at RT with Alexa Fluor-conjugated secondary antibodies (1:1000 dilution). All sections were counterstained with DAPI (ThermoFisher Scientific, Cat. D1306), and images of rat corneal samples were acquired with an Olympus IX71 fluorescent microscope.

Unbiased imaging-based evaluation of RBD binding

Twenty-four hours after Alexa 594-RBD was added to the HCEC, the cells were washed with PBS (3x/5min) and fixed with 4% paraformaldehyde for 30 minutes at RT. The HCEC were washed 2x with PBS and stained with Hoechst 33342 Solution (ThermoFisher Scientific, Cat. 62249) for 30 minutes at RT. Next, the HCEC were washed 2x with PBS before imaging. For unbiased data collection, 7 designated areas were defined in each well (Supplementary Fig. S7) and captured with an Olympus FV3000 confocal laser scanning microscopy under "Multi Area Time Lapse" (MATL) mode. All images were acquired with the same parameters and Z-section range, converted and inputted in the Imaris software version 9.5.1. The threshold for the control images was defined by the HCEC without Alexa 594-conjugated RBD of S protein and using it as a threshold filter for the Imaris batch image processing function. The sum of total intensity for each image was used to evaluate the binding efficiency. The whole process was summarized in the Supplementary Fig. S7b,c.

Droplet Digital PCR (dd-PCR)

Total RNA was isolated using RNeasy Plus Mini Kit (Qiagen, Germany), and 1 μg of total RNA was reverse transcribed using an iScript cDNA Synthesis Kit (Bio-Rad, Cat. 170–8841). For ddPCR, 10 ng of cDNA was multiplexed with *Ace2* and *phosphoglycerate kinase 1* (*Pgk1*) probes (Bio-Rad, Cat. qHSACEP005-1563 and dHSACPE503-3809) using dd-PCR Supermix for Probes No dUTP (Bio-Rad, Cat. 1863024). Then, 20 μL of the reaction was mixed with 70 μL of Droplet Generation Oil (Bio-Rad Cat:1863005) to make the reaction droplets. The emulsified samples were carefully transferred to PCR plates (Bio-Rad, Cat. 12001925) and amplified using the cycling: 95 °C for 10 minutes, 40 cycles of a two-step cycling protocol (94 °C for 30 seconds and 60 °C for 1 minute), and 98 °C for 10 minutes. Next, the post-cycling plate was placed into the QX200 Droplet Reader with the FAM/HEX setting. The absolute quantity of DNA per sample (copies/μL) was processed using QuantaSoft Analysis Pro Software. For the data analysis, the ratio of quantified *Ace2* to *Pgk1* was used.

Capillary-based Western Blot

The capillary-based western assay was performed using a Jess Protein Simple system (San Jose, CA, USA) as manufacture suggested protocol. Briefly, samples were lysed with RIPA buffer containing a

protease inhibitor cocktail (Sigma, Cat. P8340). Cell debris was removed after 10 min centrifugation at 16,000 x g. Protein concentration was determined by BCA assay (Thermo Fisher Scientific, Cat. 23225) and 1 μg used/ reaction. Fluorescent Master Mix was mixed with 40 mM DTT, and the mixture was added to each sample to provide a denaturing and reducing environment. Samples were heated at 95 °C/5 min, and 3 μL of each sample were loaded. The 12–230 kDa cartridge (Protein Simple – #SM-W004) was used. Primary antibodies were diluted in antibody diluent 2 buffer (Protein Simple, #042-203) while the working solution of secondary antibodies was provided by the company (Protein Simple, #042-206). Then, the filled plate was spin-down for 10 min at 1,000 x g to remove bubbles and plate, and capillaries were loaded into the Jess machine. For data analysis, the area of spectra that matched the molecular weight of the target protein was used. To reduce the coefficient variant, we analyzed the GAPDH for each capillary. The ratio of the targeted protein to GAPDH was used for statistical comparisons. For visualization, the artificial lanes generated from spectra volume was used.

High-throughput qPCR using Biomark™ HD

Quantitative PCR was performed with the Biomark HD system (Fluidigm, San Francisco, CA, USA). Briefly, 200 ng of RNA was reverse-transcribed using iScript Reverse Transcription Supermix (Bio-Rad), and the cDNA was pre-amplified using the PreAmp Master Mix (PN 100-5580; Fluidigm). The cDNA was then subjected to Exonuclease I treatment and diluted 5 times in TE Buffer. The qPCR reaction mixture and primer reaction mixture were made and loaded into the Biomark 96.96 IFC™ (Integrated Fluidic Circuit). The enzyme reaction was mixed using Juno™ Controller (Fluidigm) and run using the cycling program of (i) 70 °C for 40 minutes followed by 60 °C for 30 seconds, (ii) hot start for 1 minute at 95 °C, (iii) 30 cycles of denaturation at 96 °C for 5 seconds, and annealing at 60 °C for 20 seconds, and (iv) melting curves between 60 °C and 95 °C with 1 °C increments/3 seconds. The Ct value of target genes was normalized to the house-keeping genes *Gapdh*, *Hprt1*, and *Tfrc* before normalized to the vehicle group. Relative fold changes from the ΔΔCT calculation was used to make the graph. Primersequences are provided in Table 2.

Statistical analysis

Data are expressed as mean ± SD. The data were analyzed by 1-way ANOVA followed by Dunnett's multiple comparisons post hoc test at 95% confidence level with the vehicle as reference. All graphs were made using GraphPad Prism 7 (GraphPad Software, La Jolla, CA, USA) with the mean ± SD while all statistical analyses were done using built-in function of Prism 7.

Declarations

Data availability

The data that support the findings of this study are available from the corresponding authors upon reasonable request.

Author Contributions

H.E.P.B., N.G.B, and T.L.P. designed the experiments. T.L.P. performed acquisition and analysis of data, writing, and critical review of the manuscript; J.H. did the injury, treatments, isolation of rat tissues, and immunohistochemistry. A.H.K. coded and prepared the drugs, maintained the HCEC, and helped with RNA extraction. J.C. prepared Alexa 594-conjugated RBD fragment of SARS-CoV-2 Spike. K.V.D. did the HCEC RNA extraction, ddPCR analysis, and SASP Secretome (β-Gal staining) of HCEC. R.N. and

N.A.P. synthesized ELV-N32, NPD1, and RvD6i. H.E.P.B. and N.G.B supervised the study and wrote the manuscript.

Competing Interest Declaration

The authors declare no competing interests.

Additional Information

Supplementary Information is available for this paper.

Correspondence and requests for materials should be addressed to Haydee E.P. Bazan (hbazan1@lsuhsc.edu) or Nicolas G. Bazan (nbazan@lsuhsc.edu).

References

1. Naming the coronavirus disease (COVID-19) and the virus that causes it. https://who.int/emergencies/diseases/novel-coronavirus-2019/technical-guidance/naming-the-coronavirus-disease-(covid-2019)-and-the-virus-that-causes-it.

2. Zhu, N. *et al.* A Novel Coronavirus from Patients with Pneumonia in China, 2019. *Engl. J. Med.* **382**, 727–733 (2020).

3. Chen, N. *et al.* Epidemiological and clinical characteristics of 99 cases of 2019 novel coronavirus pneumonia in Wuhan, China: a descriptive study. *The Lancet* **395**, 507–513 (2020).

4. Hoffmann, M. *et al.* SARS-CoV-2 Cell Entry Depends on ACE2 and TMPRSS2 and Is Blocked by a Clinically Proven Protease Inhibitor. *Cell* **181**, 271-280.e8 (2020).

5. Hoffmann, M., Kleine-Weber, H. & Pöhlmann, S. A Multibasic Cleavage Site in the Spike Protein of SARS-CoV-2 Is Essential for Infection of Human Lung Cells. *Cell* **78**, 779-784.e5 (2020).

6. Sungnak, W. *et al.* SARS-CoV-2 entry factors are highly expressed in nasal epithelial cells together with innate immune genes. *Med.* **26**, 681–687 (2020).

7. Zhou, L. *et al.* ACE2 and TMPRSS2 are expressed on the human ocular surface, suggesting susceptibility to SARS-CoV-2 infection. *Surf.* **18**, 537–544 (2020).

8. Panigrahy, D. *et al.* Inflammation resolution: a dual-pronged approach to averting cytokine storms in COVID-19? *Cancer Metastasis Rev.* (2020) doi:10.1007/s10555-020-09889-4.

9. Regidor, P.-A. Covid-19 management with inflammation resolving mediators? Perspectives and potential. *Hypotheses* **142**, 109813 (2020).

10. Serhan, C. N. Pro-resolving lipid mediators are leads for resolution physiology. *Nature* **510**, 92–101 (2014).

11. Bazan, N. G. Docosanoids and elovanoids from omega-3 fatty acids are pro-homeostatic modulators of inflammatory responses, cell damage and neuroprotection. *Aspects Med.* **64**, 18–33 (2018).

12. Serhan, C. N., Hamberg, M. & Samuelsson, B. Lipoxins: novel series of biologically active compounds formed from arachidonic acid in human leukocytes. *Natl. Acad. Sci.* **81**, 5335–5339 (1984).

13. Mukherjee, P. K., Marcheselli, V. L., Serhan, C. N. & Bazan, N. G. Neuroprotectin D1: a docosahexaenoic acid-derived docosatriene protects human retinal pigment epithelial cells from oxidative stress. *Natl. Acad. Sci. U. S. A.* **101**, 8491–8496 (2004).

14. Pham, T. L. *et al.* Novel RvD6 stereoisomer induces corneal nerve regeneration and wound healing post-injury by modulating trigeminal transcriptomic signature. *Rep.* **10**, 1–12 (2020).

15. Jun, B. *et al.* Elovanoids are novel cell-specific lipid mediators necessary for neuroprotective signaling for photoreceptor cell integrity. *Rep.* **7**, 5279 (2017).

16. Do, K. V. *et al.* Elovanoids counteract oligomeric β-amyloid-induced gene expression and protect photoreceptors. *Natl. Acad. Sci. U. S. A.* **116**, 24317–24325 (2019).

17. Ziegler, C. G. K. *et al.* SARS-CoV-2 Receptor ACE2 Is an Interferon-Stimulated Gene in Human Airway Epithelial Cells and Is Detected in Specific Cell Subsets across Tissues. *Cell* **181**, 1016- 1035.e19 (2020).

18. Li, Y. *et al.* The MERS-CoV receptor DPP4 as a candidate binding target of the SARS-CoV-2 *iScience* (2020) doi:10.1016/j.isci.2020.101160.

19. Wu, P. *et al.* Characteristics of Ocular Findings of Patients With Coronavirus Disease 2019 (COVID-19) in Hubei Province, China. *JAMA Ophthalmol.* (2020) doi:10.1001/jamaophthalmol.2020.1291.

20. Huang, C. *et al.* Clinical features of patients infected with 2019 novel coronavirus in Wuhan, *Lancet Lond. Engl.* **395**, 497–506 (2020).

21. Pedersen, S. F. & Ho, Y.-C. SARS-CoV-2: a storm is raging. *Clin. Invest.* **130**, 2202–2205 (2020).

22. Sotozono, C. *et al.* Cytokine expression in the alkali-burned cornea. *Eye Res.* **16**, 670–676 (1997).

23. Coppé, J.-P., Desprez, P.-Y., Krtolica, A. & Campisi, J. The Senescence-Associated Secretory Phenotype: The Dark Side of Tumor Suppression. *Rev. Pathol.* **5**, 99–118 (2010).

24. Identification of SARS-CoV2-mediated suppression of NRF2 signaling reveals a potent antiviral and anti-inflammatory activity of 4-octyl-itaconate and dimethyl fumarate. (2020) doi:10.21203/rs.3.rs-31855/v1.

25. Yang, Y. *et al.* Plasma IP-10 and MCP-3 levels are highly associated with disease severity and predict the progression of COVID-19. *Allergy Clin. Immunol.* **146**, 119-127.e4 (2020).

26. Marten, N. W. & Zhou, J. The Role of Metalloproteinases in Corona Virus Infection. *Models Mult. Scler.* 839–848 (2005) doi:10.1007/0-387-25518-4_48.

27. Ueland, T. *et al.* Distinct and early increase in circulating MMP-9 in COVID-19 patients with respiratory failure. *Infect.* (2020) doi:10.1016/j.jinf.2020.06.061.

28. Bose, P., Bathri, R., Kumar, L., Vijayan, V. K. & Maudar, K. K. Role of oxidative stress & transient receptor potential in chronic obstructive pulmonary disease. *Indian J. Med. Res.* **142**, 245–260 (2015).

29. Luan, J., Lu, Y., Gao, S. & Zhang, L. A potential inhibitory role for integrin in the receptor targeting of SARS-CoV-2. *Infect.* (2020) doi:10.1016/j.jinf.2020.03.046.

30. Sigrist, C. J., Bridge, A. & Le Mercier, P. A potential role for integrins in host cell entry by SARS- CoV-2. *Antiviral Res.* **177**, 104759 (2020).

31. Beddingfield, B. *et al.* The Integrin Binding Peptide, ATN-161, as a Novel Therapy for SARS-CoV-2 Infection. *bioRxiv* (2020) doi:10.1101/2020.06.15.153387.

32. Samuel, C. E. Antiviral Actions of Interferons. *Microbiol. Rev.* **14**, 778–809 (2001).

33. Han, H. *et al.* Profiling serum cytokines in COVID-19 patients reveals IL-6 and IL-10 are disease severity predictors. *Microbes Infect.* **9**, 1123–1130 (2020).

34. Coronavirus Disease 2019 (COVID-19). *Centers for Disease Control and Prevention* https://www.cdc.gov/coronavirus/2019-ncov/need-extra-precautions/people-at-increased-risk.html (2020).

35. Krummel, M. F. *et al.* Paracrine costimulation of IFN-γ signaling by integrins modulates CD8 T cell differentiation. *Natl. Acad. Sci. U. S. A.* **115**, 11585–11590 (2018).

36. Schmid, M., Gemperle, C., Rimann, N. & Hersberger, M. Resolvin D1 Polarizes Primary Human Macrophages toward a Proresolution Phenotype through GPR32. *Immunol. Baltim. Md 1950* **196**, 3429–3437 (2016).

37. He, J., Pham, T. L., Kakazu, A. & Bazan, H. E. P. Recovery of Corneal Sensitivity and Increase in Nerve Density and Wound Healing in Diabetic Mice After PEDF Plus DHA Treatment. *Diabetes* **66**, 2511–

2520 (2017).

38. Pham, T. L. *et al.* Defining a mechanistic link between pigment epithelium-derived factor, docosahexaenoic acid, and corneal nerve regeneration. *Biol. Chem.* **292**, 18486–18499 (2017).

39. Liao, Y., Smyth, G. K. & Shi, W. The Subread aligner: fast, accurate and scalable read mapping by seed-and-vote. *Nucleic Acids Res.* **41**, e108 (2013).

40. Liao, Y., Smyth, G. K. & Shi, W. featureCounts: an efficient general purpose program for assigning sequence reads to genomic features. *Oxf. Engl.* **30**, 923–930 (2014).

41. Love, M. I., Huber, W. & Anders, S. Moderated estimation of fold change and dispersion for RNA-seq data with DESeq2. *Genome Biol.* **15**, 550 (2014).

42. Kuleshov, M. V. *et al.* Enrichr: a comprehensive gene set enrichment analysis web server 2016 update. *Nucleic Acids Res.* **44**, W90-97 (2016).

43. Zhou, G. *et al.* NetworkAnalyst 3.0: a visual analytics platform for comprehensive gene expression profiling and meta-analysis. *Nucleic Acids Res.* **47**, W234–W241 (2019).

44. Sharma, G. D., Kakazu, A. & Bazan, H. E. P. Protein kinase C alpha and epsilon differentially modulate hepatocyte growth factor-induced epithelial proliferation and migration. *Eye Res.* **85**, 289–297 (2007).

Tables

Table 1: List of primary antibodies used in this study

No.	Name	Company	Cat. Number	Immunofluorescence	Western Blot
1	Rabbit anti-ACE2	Abcam	Ab108252	1:1000	1:100
2	Rabbit anti-DPP4	Abcam	Ab129060	1:500	1:100
3	Rabbit anti-FURIN	Abcam	Ab183495	1:1000	1:100
4	Rabbit anti-TMPRSS2	Abcam	Ab109131	1:1500	1:100
5	Rabbit anti-GAPDH	Santa Cruz	Sc-25778		1:1000
6	Anti-neutrophil	LSBio	LS-C348005	1:500	
7	Mouse anti-rat CD68	Bio-Rad	MCA341GA	1:1000	

Table 2. Primers for qPCR

Gene name	Forward	Reverse
Ace2	CATTGGAGCAAGTGTTGGATCTT	GAGCTAATGCATGCCATTCTCA
Cdkn2a	GGGGGCACCAGAGGCAGT	GGTTGTGGCGGGGGCAGTT
Mmp1	GGGCTTGAAGCTGCTTACGAATT	CAGCATCGATATGCTTCACAGTTCT
Gapdh	TGGACCTGACCTGCCGTCTA	CCCTGTTGCTGTAGCCAAATTC
Tfrc	GGCTACTTGGGCTATTGTAAAGG	CAGTTTCTCCGACAACTTTCTCT
Hprt1	GACCAGTCAACAGGGGACAT	AACACTTCGTGGGGTCCTTTTC

Figures
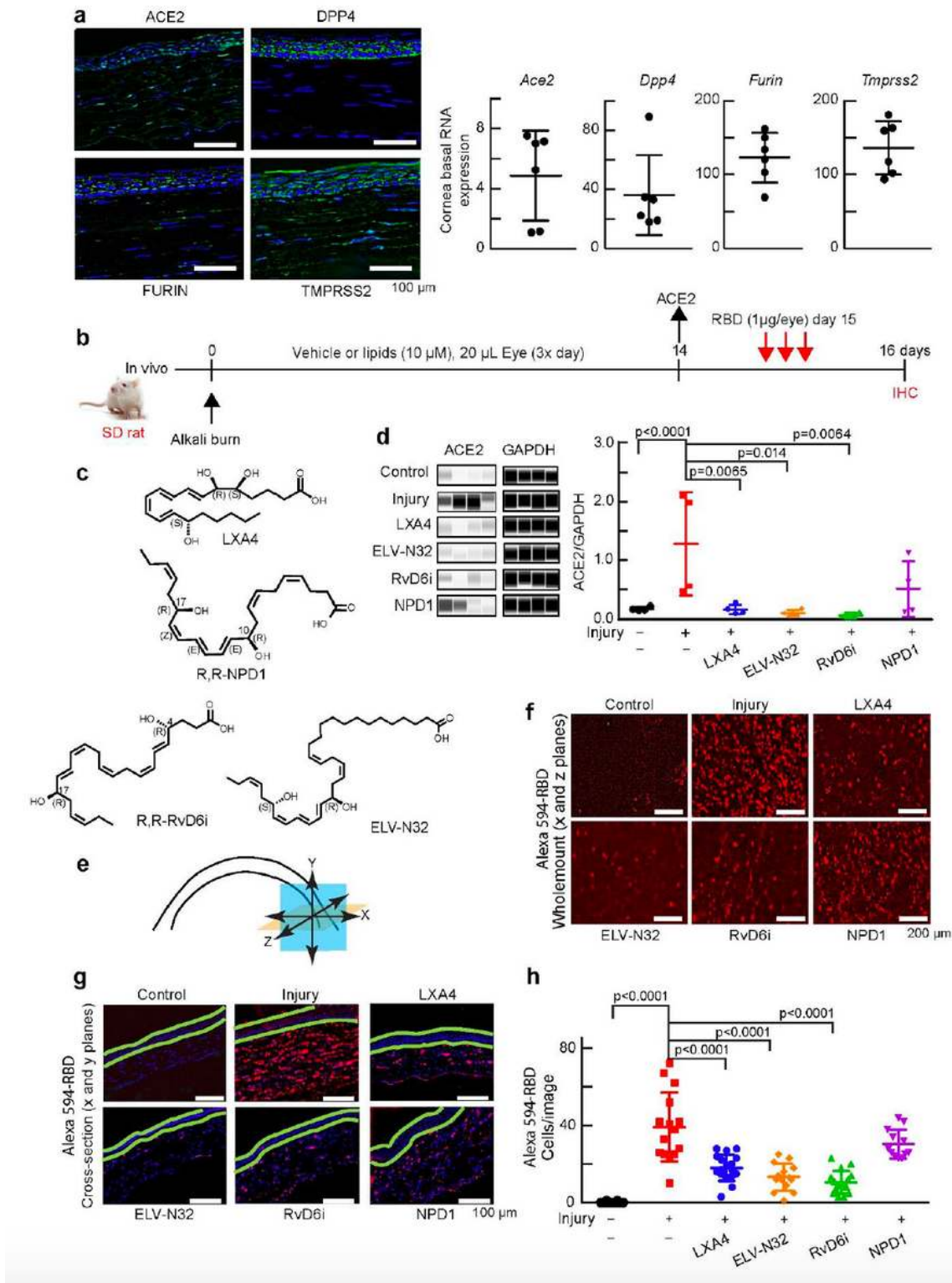
Figure 1

Selective lipid mediators reduce cornea injury-induced expression of ACE2 and binding of Alexa 594-RBD. a, Expression of Ace2, Dpp4, furin and Tmprss2 in the uninjured rat cornea. Left: representative immunofluorescence imaging. DAPI stains nuclei (blue). Immunofluorescence shows ACE2 expressed in the epithelium and stroma. Right: RNA-seq data. b, Experimental design. After alkali burn, rats received eye drops of lipid mediators or vehicle 20 μl/eye, 3 times/day for 14 days (double- blinded). ACE2

expression was assayed at day 14 after injury +/- lipids treatment. At day 15, rats were treated with Alexa 594-RBD (1 μg/eye, 3 times) and corneas examined a day later. c, Lipid mediators studied. The chirality in all figures of RvD6i and NPD1 used in this study had the R,R stereochemistry. d, ACE2 abundance before and after injury +/- lipids using Jess capillary-based Western Blot system (Protein Simple). ACE2 densitometry normalized to GAPDH in the same capillary to minimize errors. Data is from one rat cornea for each data point (N = 4). The p-values of ANOVA-post hoc Dunnett's multiple comparisons test with vehicle as reference are shown. Mean and SD are depicted as the lines. e, Illustration showing corneal analysis by wholemount (x and z planes – orange color) and cross-section (x and y planes – blue color). f, Wholemount images of binding of Alexa 594-RBD in corneas after injury and treatments. The control cornea (no-injury) has very low Alexa 594-RBD signal, while the injured cornea shows intense fluorescence. LXA4, ELV-N32, and RvD6i decrease Alexa 594-RBD binding while NPD1 fails. g, Cross-section images of the same corneas shown in f. The green lines were added to separate the epithelium from the stroma. Most of Alexa 594-RBD signal was found in the stroma. h, Quantification of Alexa 594-RBD positive cells. Each data point represents number of cells/cross-section image. Values are means ±SD and p-values calculated by ANOVA-post hoc Dunnett's multiple comparisons test with vehicle as reference (4 images/cornea and 4 rat corneas/condition). The map of image capture is shown in Supplementary Fig. S1.
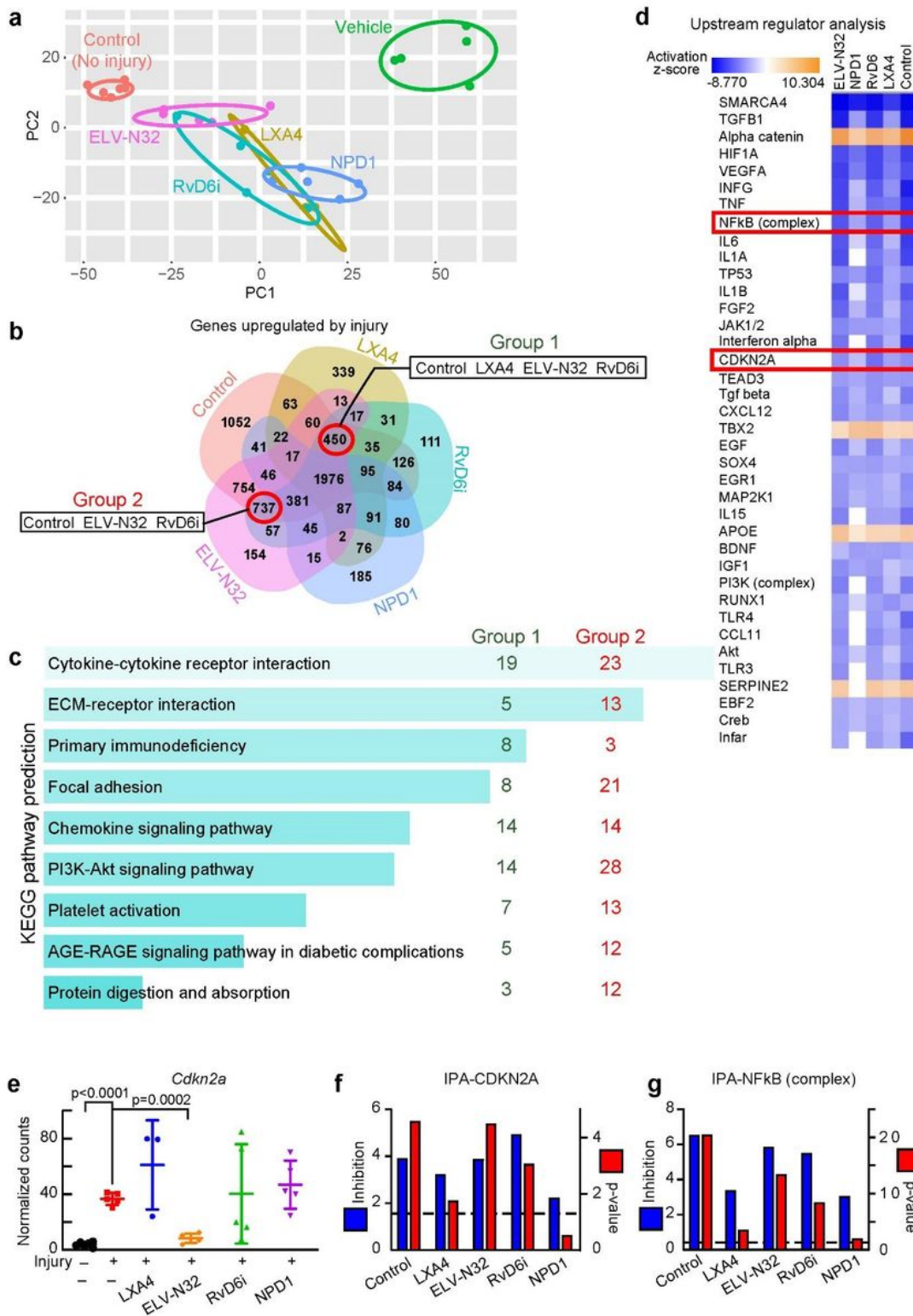
Figure 2

Selective lipid mediators disrupt ACE2 upregulation and injury-mediated hyper- inflammation, senescence, and cytokine storm components. a, PCA plot of RNA-seq data. Rat corneas were analyzed at day 14 after injury +/- treatments (Fig. 1b). Each data point represents one animal (N = 5/group, except LXA4 with N = 3 and control with N = 6). The eclipse of 95% confidence interval was used to group data points from the same set of treatment. b, Venn diagram of significant genes (FDR < 0.05) upregulated by the vehicle

treatment of injured corneas (RNA-seq data set was analyzed using DEseq2 with vehicle injured corneas as reference). The negative log2 fold change genes (upregulated by vehicle) with FDR < 0.05 were used. We excluded NPD1 because it failed to decrease Ace2 expression upon injury (Fig. 1d). The groups of shared genes between control-LXA4-ELV-N32-RvD6i and control- ELV-N32-RvD6i are depicted. c, The KEGG-pathway enrichment networks of selected genes from b. Bars were sorted by p-value. The length of the bar represents the significance of the pathway, while the lighter the color, the higher the significance. The number shows amount of genes from denoted group that are enriched in each pathway. d, IPA upstream regulator analysis of significant genes vs. vehicle (injury) group. There are proteins with negative activation z-score compared to vehicle group (blue color). Among those are CDKN2A and NFkB (complex). e, RNA-seq normalized counts of Cdkn2a gene that encodes the senescence key-marker p16INK4a; ELV-N32 decrease its expression. Data correspond to one cornea for each data point and is presented as mean ±SD. The p-values were analyzed by ANOVA-post hoc Dunnett's multiple comparisons test with vehicle as reference. The normalized counts were used for analysis. IPA scores for CDKN2A (f) and NFkB (complex) (g) upstream regulators. The left y-axis is the inhibition z-score, while the right y-axis e is -log10 of p-value. The cutoff line for p-value is <0.05.
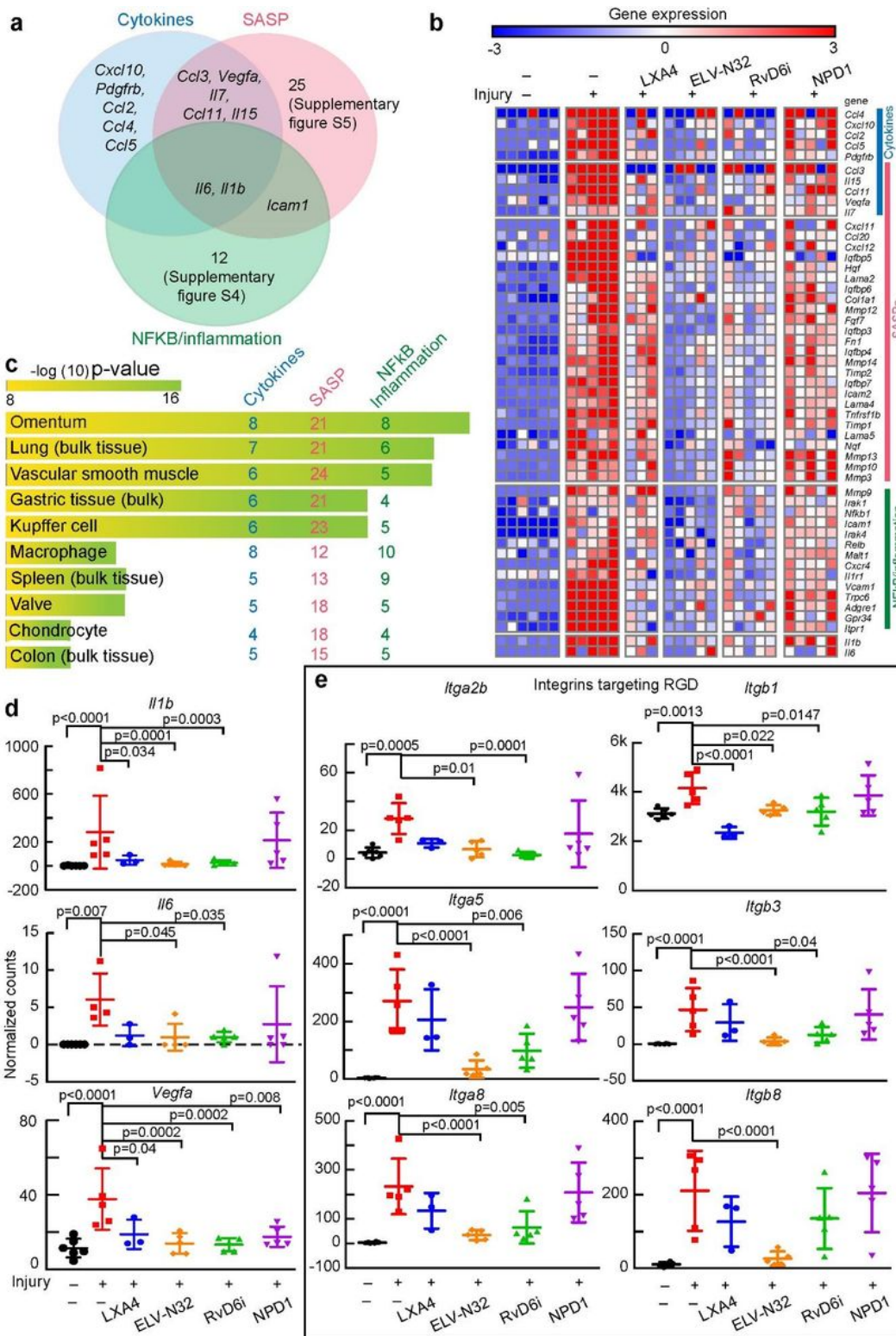
Figure 3

Lipid mediators down-regulate injury-induced gene expression of NFkB/inflammation, senescence-associated secretory phenotype, and cytokine storm markers after cornea injury. a, Venn diagram of cytokines, SASP, and NFkB inflammatory genes upregulated by injury. b, Heatmap of normalized counts data. Each small square represents data from one cornea. There are 51 genes increased by injury, and most are inhibited by ELV-N32 and RvD6i treatment. c, The ArchS4 human tissue analysis prediction for

the 51 genes. The length of the bar represents the significance of the gene set in the tissues, while the lighter the color, the higher the significance. The number shows the amount of genes from the denoted group enriched in each pathway. d, Scatter plots of Il1b, Il6, and Vegfa genes. e, Scatter plots of genes that encode proteins that target RGD. The p-value of ANOVA-post hoc Dunnett's multiple comparisons test with vehicle as reference are shown. Mean and SD are depicted as the lines. The normalized counts were used for analysis.
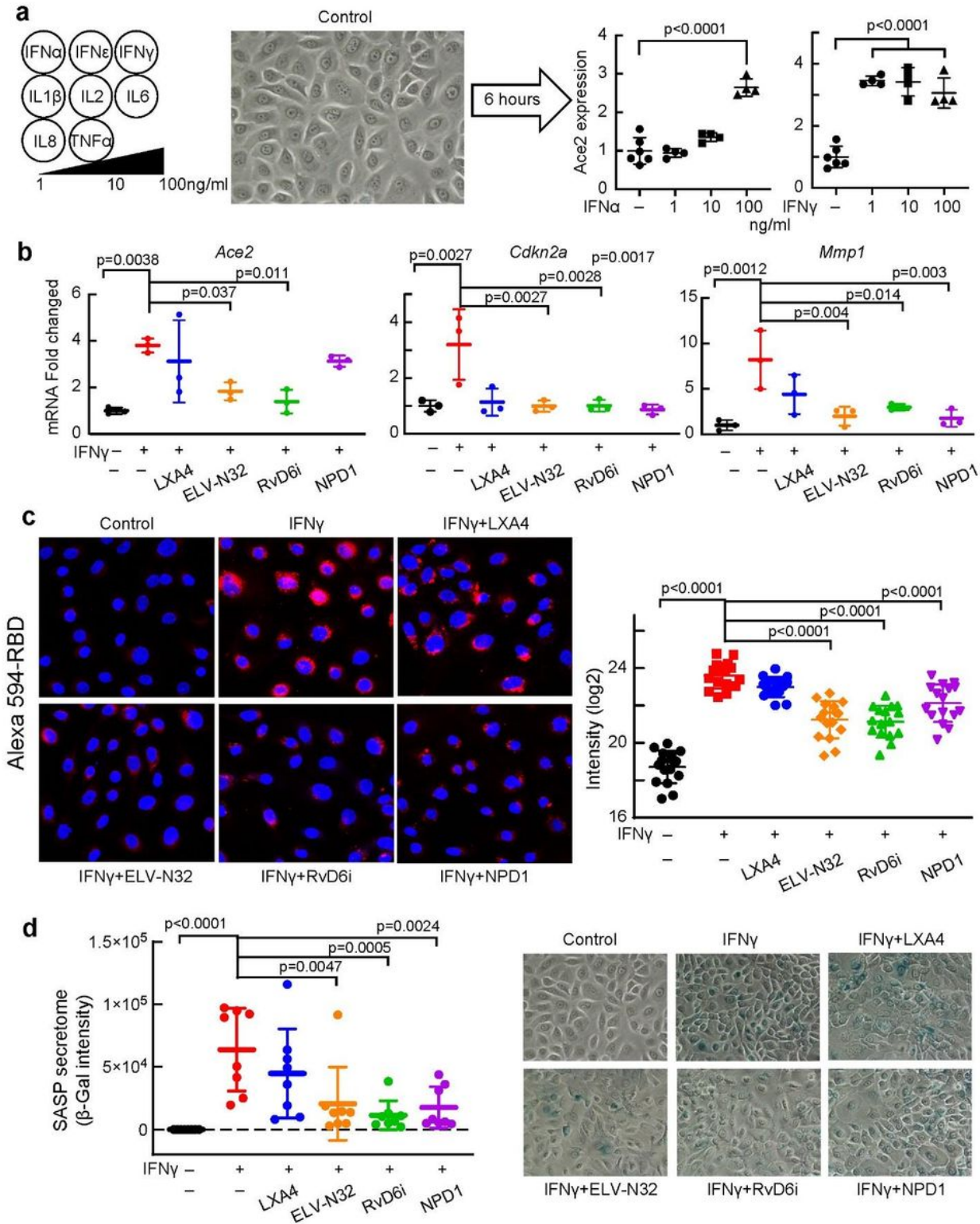

Figure 4

Lipid mediators attenuate IFNγ-induced ACE2 expression, senescence programming, and binding of Alexa 594-RBD in human corneal epithelial cells (HCEC). a, Among several cytokines tested only IFNγ and α, induces ACE2 expression in HCEC (6 hours after stimulation, analyzed by dd- PCR). b, Effect of lipid mediators on gene expression of Ace2, Cdkn2a, and Mmp1 of HCEC after adding IFNγ (100 ng/ml). ΔΔCT normalized fold change was used. p-values of statistical t-test analysis in comparison to vehicle group are shown. Mean and SD are shown as the lines. c, Alexa 594-RBD binding in HCEC. IFNγ (100 ng/ml) and lipid mediators (200 nM) were added to the HCEC for 12 h. Alexa 594- RBD (0.5 ng/well) was then added and images taken 24 h after. Fifteen images/condition analyzed. Representative images are shown (left side), and the Imaris based calculation was plotted (right-hand side). Data are presented as single image/each data point. The p-value of ANOVA-post hoc Dunnett's multiple comparisons test with vehicle as reference. Mean and SD are shown as the lines. d, SASP Secretome (β-Gal staining) of HCEC 24 h after IFN-γ challenge and +/- lipid mediators. Each point represents one image. The p-value of ANOVA-post hoc Dunnett's multiple comparisons test with vehicle as reference are shown. Mean and SD are shown as the lines. Representative images for each condition are in the right panel.

Supplementary Files

This is a list of supplementary files associated with this preprint. Click to download.

- SupplementalFigures.pdf